

RESEARCH ARTICLE | DECEMBER 23 2024

Distinct deformation mechanisms of silicate glasses under nanoindentation: The critical role of structure

Special Collection: [Disordered Materials at the Atomic Scale](#)

Ziming Yan; Ranran Lu; Linfeng Ding  ; Lianjun Wang ; Zhen Zhang  

 Check for updates

J. Appl. Phys. 136, 245101 (2024)

<https://doi.org/10.1063/5.0244335>



View
Online



Export
Citation

Articles You May Be Interested In

Understanding the response of aluminosilicate and aluminoborate glasses to sharp contact loading using molecular dynamics simulation

J. Appl. Phys. (July 2020)

Revealing the atomic-scale origin of simultaneously enhanced hardness and crack resistance in a single phase material

J. Appl. Phys. (April 2021)

Nanoscale plasticity in titania densified alumina ceramics

J. Appl. Phys. (April 2022)

Distinct deformation mechanisms of silicate glasses under nanoindentation: The critical role of structure



Cite as: J. Appl. Phys. 136, 245101 (2024); doi: 10.1063/5.0244335

Submitted: 17 October 2024 · Accepted: 4 December 2024 ·

Published Online: 23 December 2024



View Online



Export Citation



CrossMark

Ziming Yan,¹ Ranran Lu,¹ Linfeng Ding,^{1,a)} Lianjun Wang,¹ and Zhen Zhang^{2,a)}

AFFILIATIONS

¹State Key Laboratory for Modification of Chemical Fibers and Polymer Materials, Engineering Research Center of Advanced Glass Manufacturing Technology, Ministry of Education, Donghua University, Shanghai 201620, China

²Department of Physics, Chengdu University of Technology, Chengdu 610059, China

Note: This paper is part of the special topic on Disordered Materials at the Atomic Scale.

a) Authors to whom correspondence should be addressed: linfeng.ding@dhu.edu.cn and zhen.zhang@cdut.edu.cn

ABSTRACT

We use large-scale molecular dynamics simulations to investigate the indentation response of three silica-based glasses with varying compositional complexities. Our primary goal is to clarify the roles of the typical network-modifying species, namely, sodium, and the secondary network-forming species, namely, boron, in influencing the mechanical behavior of the glasses under localized stress. The distinct mechanical responses of the glasses are linked to structural features such as bond strength, network connectivity, and atomic packing density. The enhanced nanoscale ductility of sodium silicate and sodium borosilicate glasses, compared to silica, is attributed to the structural flexibility induced by Na atoms, which depolymerize the network, and by B species in mixed coordination. We also find that shear flow, driven by network flexibility, is the dominant deformation mechanism in the sodium silicate and sodium borosilicate glasses, while densification dominates in silica due to its low packing density. The evolution of short-to-intermediate-range structures is responsible for the distinct deformation behaviors of the glasses. These results highlight the critical role of structure in determining the deformation mechanisms of silicate glasses under sharp contact loads, providing insights for improving the mechanical performance of these materials.

© 2024 Author(s). All article content, except where otherwise noted, is licensed under a Creative Commons Attribution (CC BY) license (<https://creativecommons.org/licenses/by/4.0/>). <https://doi.org/10.1063/5.0244335>

24 December 2024 00:39:22

I. INTRODUCTION

Silicate glasses are disordered materials with diverse applications, including construction, packaging, electronics, and optics.¹ These materials are used for their desired properties such as transparency and chemical stability, but their inherent brittleness can limit their use in critical applications, such as high-stress environments like aerospace or architecture. Therefore, a fundamental understanding of their mechanical properties (e.g., strength and toughness) and deformation mechanisms is essential for improving their mechanical reliability for practical applications.² Among the techniques for investigating the mechanical properties of glasses, indentation is indispensable due to its ability to induce permanent deformation in a controlled manner.³

Glass deformation under a sharp contact load can be classified into elastic deformation, inelastic deformation, and cracking.³ Inelastic deformation has been recognized as a critical stage that determines the overall mechanical performance of glass. Numerous experimental and computational studies have identified densification and isochoric shear flow as the two primary mechanisms of inelastic deformation in silicate glasses.^{4–20} Densification is mainly manifested as the sink-in beneath the contact surface, with its extent strongly depending on properties such as atomic packing density (C_g) and Poisson's ratio (ν).^{3,21,22} On the other hand, shear deformation may occur in the form of pileup above the contact surface and/or shear banding, depending on the glass's chemical composition.^{3,23} For example, Januchta and Smedskjaer²² showed

that the chemical composition directly impacts the indentation response of oxide glasses. Notably, the coordination number of triangular boron atoms can increase to four under compressive stress, making boron-rich glasses more prone to densification than boron-free glasses. Duan *et al.*²⁴ found that the subsurface densification in soda lime silicate glasses depends more strongly on the indentation rate than shear flow. A recent experimental study using a sharp indenter on a series of silicate glasses revealed that, far from the indent, a new elevated volume (called lift-up) forms in addition to the pileup region near the indent, indicating that glass deformation behavior also depends on the indenter shape.²⁵

Alongside experimental studies, computer modeling and simulations have been crucial in offering microscopic insights into the mechanical response of silicate glasses under indentation. For example, early molecular dynamics (MD) simulations by Nomura *et al.*¹⁴ demonstrated that defect migration and recombination are key contributors to structural changes during nanoindentation. Kilymis *et al.*^{7,8,26,27} later showed that irradiation-induced structural disorder alters the densification and shear flow patterns of borosilicate glasses. Luo *et al.*¹² introduced a crack nucleation criterion for glasses, highlighting its relevance to impact indentation. More recently, Liu *et al.*¹¹ explored how chemical composition affects the indentation response of glass, showing that aluminosilicate and aluminoborate glasses exhibit distinct responses due to differences in the atomic structure. By studying the indentation response of model metallic glasses, Liu *et al.*²⁸ observed a distinct region above the contact surface, consistent with experimental findings from Refs. 25 and 29–31. Our recent work using large-scale MD simulations demonstrated how densification, shear deformation, and atomic migration contribute to the mechanical response of a sodium silicate glass during nanoindentation.³²

Despite these advancements, the fundamental atomic-level mechanisms of inelastic deformation during nanoindentation in silicate glasses, especially the influence of structure, remain poorly understood. Closing this knowledge gap requires higher-resolution experimental studies and reliable modeling and simulation methods to capture both the short-term/localized events and cumulative deformation behaviors. In this study, we use large-scale MD simulations to systematically investigate the indentation response of three representative silicate glasses. The primary objective is to understand how network-modifying species (modifier) and secondary network-forming species alter the way the glass responds to a sharp contact loading and the underlying atomic-scale mechanisms. These microscopic insights are crucial for understanding the deformation behavior of multi-component silicate glasses and for improving the mechanical performance of these disordered materials.

II. SIMULATION DETAILS

We performed classical MD simulations on three systems: SiO₂, Na₂O–3SiO₂ (hereafter denoted as NS3), and Na₂O–B₂O₃–2SiO₂ (hereafter denoted as NBS2), which are prototypical oxide glass-formers with broad scientific and industrial significance.¹ The increasing chemical complexity from silica to NS2 to NBS2 also allowed us to explore the role of the network modifier (Na) as

well as the secondary network-forming species (B) in influencing the structure and mechanical properties of the glasses. The interaction between the atoms was described by a two-body effective potential recently proposed by Sundararaman *et al.*^{33–35} Its functional form is given by

$$V(r_{\alpha\beta}) = \frac{q_\alpha q_\beta e^2}{4\pi\epsilon_0 r_{\alpha\beta}} + A_{\alpha\beta} \exp(-r_{\alpha\beta}/B_{\alpha\beta}) - \frac{C_{\alpha\beta}}{r_{\alpha\beta}^6}, \quad (1)$$

where $r_{\alpha\beta}$ is the distance between two atoms of species α and β . q_α is the effective charge of species α . $A_{\alpha\beta}$, $B_{\alpha\beta}$, and $C_{\alpha\beta}$ are potential parameters. In order to achieve high computational efficiency, the long-range interactions were evaluated using the method proposed by Wolf *et al.*,³⁶ where the long-range cutoff was set to 10 Å. This potential was parameterized using data from both *ab initio* simulations and compression experiments as reference. More details of this potential and the values of the potential parameters can be found in Refs. 33–35. This potential has been shown to reliably describe the structural, mechanical, and surface properties of multi-component silicate glasses,^{11,37–40} all relevant to the glass's response under sharp contact loading. Therefore, MD simulations using this interaction potential are expected to provide valuable atomistic insights into the origin of the distinct deformation behaviors of the three glasses under indentation.

The simulation procedures for producing the glasses as well as the subsequent mechanical tests were similar to our previous study.³² First, we produced bulk glass samples using a melt-quench procedure. The initial box, containing around 5000 atoms, had a side length of around 4 nm, determined according to the experimental glass densities.⁴¹ The sample was first melted and equilibrated at 3600, 3000, and 2100 K for silica, NS3, and NBS2, respectively. Subsequently, the liquid samples were cooled down to 300 K using a constant rate of 1 K/ps, followed by an annealing stage at 300 K for 125 ps, resulting in three bulk glasses. Figure 1 shows their representative atomic configurations. All simulations were done in the isothermal-isobaric ensemble at zero pressure.

Next, we carried out uniaxial tensile simulations for the bulk glasses. Specifically, the glass samples were elongated at a constant strain rate of 0.5 ns⁻¹ along the x direction until fracture (i.e., the tensile stress drops to zero), whereas zero stress was kept in the other two axial directions. All simulations were performed using the isothermal-isobaric ensemble at zero pressure with periodic boundary conditions applied in all axial directions. The integration time step was chosen to be 1.0 fs.

The stress-strain (σ - ε) curves as obtained from the tensile simulations were linearly fitted in the range $\varepsilon = 0$ –0.001 to calculate the Young modulus (E). The Poisson ratio (ν) was calculated by linearly fitting the transverse strain vs axial strain curve in the strain range $\varepsilon = 0$ –0.01. The shear modulus (G) and the bulk modulus (K) were calculated following Ref. 41. The mass density, number density, and calculated elastic properties are given in Table I.

Before performing nanoindentation simulation, we first replicated the 5000 atom bulk glass samples to produce large samples with a thin slab geometry; i.e., the dimensions in the x , y , and z directions were approximately 145, 75, and 4 nm, respectively.

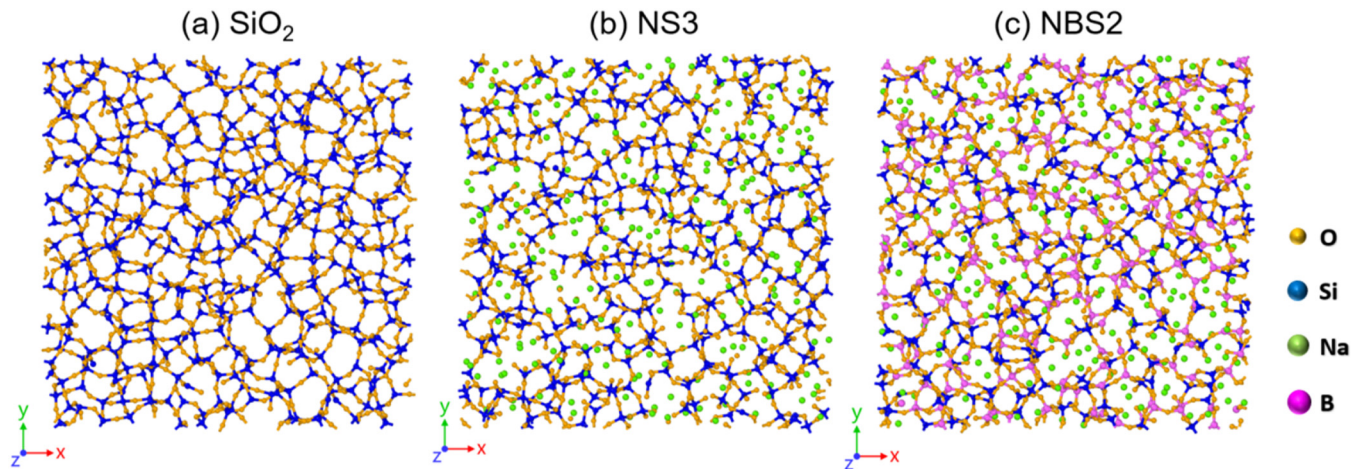


FIG. 1. Slices of the atomic configurations of the three bulk glasses at 300 K. O, Si, Na, and B atoms are represented by balls in yellow, blue, green and pink, respectively. Si–O and B–O bonds are determined using a cutoff of 2.0 Å and are shown to indicate the polymerized network. Each slice has a thickness of 1 nm.

The large samples were subsequently heated up to 600 K for 160 ps to allow adequate structural reorganization before cooling them down to 300 K at a constant rate of 1 K/s. Previous studies have shown that this procedure allows to significantly mitigate the influence of the periodic boundaries on the mechanical response of the glass while significantly reducing the computational cost.^{28,44}

Nanoindentation simulations of the glasses were done following the work of Huang and coworkers^{11,28,45} and our previous study.³² The geometry of the indenter was controlled by the indenter angle θ and the indenter tip radius R . We have chosen the indenter angle $\theta = 35.3^\circ$ to match the geometry of the sharp indenter used in a recent experimental study.²⁵ The tip radius R was set to 0.1 nm. The periodic boundary condition in the y direction was released to create a free surface on the top, whereas the bottom layer with a thickness of 1 nm was fixed. The interaction between atoms and the indenter was defined by a spring constant of 32 GPa. During the loading and unloading processes, the indenter moved vertically along the y direction at a constant speed of 50 m/s. At the maximum indentation depth of 25 nm, the indenter was held for 125 ps, which is sufficiently long to ensure force convergence. To improve the statistics of the results, we performed parallel indentation tests at three different positions for each glass.

III. RESULTS AND DISCUSSION

A. Mechanical properties of the bulk glasses

To better understand the mechanical response of the glasses under nanoindentation, we first discuss the mechanical properties of the bulk glasses. Table I shows that the simulated glass densities as well as the elastic moduli agree well with experimental data,^{41–43} giving confidence in further investigating the mechanical response of the glasses under indentation. We find that the B atoms in the NBS2 glass are in mixed coordination with 52% of them being fourfold coordinated. This proportion is slightly lower than the experimentally reported value of 58%–64% based on ¹¹B MAS NMR for the same glass composition.^{46–49} The difference between the two results may arise from the uncertainties in experimental measurements and/or the difference in the cooling rate used in experiments and simulations.

Table I also reveals that silica and NBS2 have similar values for E and G , despite their structural differences. This can be rationalized by considering that elastic moduli primarily depend on the bond strength density ρ_{bs} , which is given by $\rho_{bs} = \rho_{\text{SiO}}^N \gamma_{\text{SiO}} + \rho_{\text{BO}}^N \gamma_{\text{BO}} - \rho_{\text{NaO}}^N \gamma_{\text{NaO}}$, where ρ_{SiO}^N denotes the number density of the SiO bond and γ_{SiO} is the SiO bond strength (dissociation energy).^{50,51} We find that for silica, NS3,

24 December 2024 00:39:22

TABLE I. Composition, elastic moduli, densities, and the fraction of bridging oxygen of the simulated bulk glasses. Values in parenthesis are experimental data from Refs. 41–43.

| Glass | Composition | Young's modulus, E (GPa) | Bulk modulus, K (GPa) | Shear modulus, G (GPa) | Poisson's ratio, ν | Mass density, ρ (g/cm ³) | Atomic packing density, C_g (g/cm ³) | Bridging oxygen (%) |
|------------------|---|----------------------------|-------------------------|--------------------------|------------------------|---|--|---------------------|
| SiO ₂ | 100%SiO ₂ | 73.1 (72.7) | 37.6 (36.4) | 31.1 (31.2) | 0.18 (0.17) | 2.20 (2.20) | 0.387 | 99.6 |
| NS3 | 75SiO ₂ –25Na ₂ O | 56.3 (60) | 36.1 (37) | 22.7 (24) | 0.24 (0.23) | 2.46 (2.43) | 0.451 | 71.6 |
| NBS2 | 50SiO ₂ –25Na ₂ O–25B ₂ O ₃ | 72.7 (76.2) | 43.3 (47.7) | 29.8 (30.8) | 0.22 (0.23) | 2.56 (2.53) | 0.502 | 86.2 |

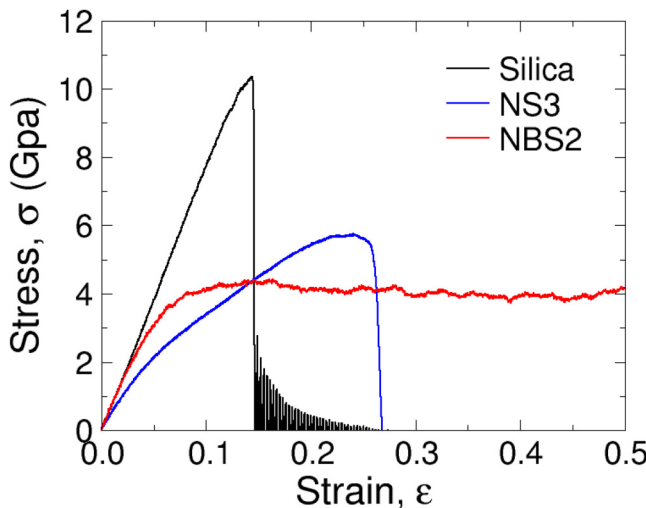


FIG. 2. Stress–strain (σ – ϵ) curves for the three bulk glasses under uniaxial tension.

and NBS2, the ρ_{bs} values are 39.7, 31.1, and 38.1 kJ/(mol $\times \text{Å}^3$), respectively. Remarkably, the ratio between these values aligns closely with E and G in Table I, indicating that the bond strength density governs the elastic properties of the glasses.

Poisson's ratio, often considered a key factor in controlling the deformation and cracking behaviors across a wide range of materials,⁵² does not appear to reflect the compositional change from NS3 to NBS2. In contrast, changes in the chemical composition more strongly affect the network connectivity, as reflected by the concentration of bridging oxygen (BO, i.e., oxygen bonded with two or more Si/B), and the atomic packing density (C_g , i.e., the number of atoms per unit volume), both of which are expected to influence the glass's response to stress.

The differences in the mechanical properties of the three glasses are evident not only at small strains, i.e., pertaining to elastic properties, but also at large strains. Figure 2 plots the stress–strain (σ – ϵ)

curves for the three bulk glasses under uniaxial tension. Silica exhibits its typical brittle behavior in that the σ – ϵ curve shows a nearly linear increase without notable softening up to the maximum strength, after which the stress drops instantly to zero. In contrast, the NS3 glass shows significant softening at $\epsilon \sim 5\%$ and fails at $\epsilon \sim 22\%$, much higher than silica, indicating that the addition of the network modifier Na increases the glass's deformability.

Remarkably, the NBS2 glass exhibits super nano-ductility, showing homogeneous flow at $\epsilon > 10\%$ and no fracture even at $\epsilon = 50\%$, indicating that the inclusion of B significantly enhances the deformation ability of the glass. (We note that this super nano-ductility is an intrinsic property of the glass, with a nearly defect-free structure and deformed under very high strain rates, in contrast with mechanical tests performed on glasses in experiments.) Therefore, it can be concluded that the glass's nano-ductility increases with chemical complexity (and corresponding structural flexibility), consistent with the findings of Wang *et al.*⁵³ We note that although silica and NBS2 have comparable elastic moduli, which as mentioned above is mainly determined by the bond strength density, plasticity primarily depends on the ability of the structure to rearrange upon deformation.

To further understand the distinct stress–strain behaviors of the three glasses, we have tracked the bond switching activities (i.e., change of local coordination) of the three cations. By comparing the coordination of the atoms in the deformed configurations with the initial configuration ($\epsilon = 0$), we determined three types of coordination changes of the atoms, namely, coordination number increased, coordination number decreased, and coordination number unchanged but the neighboring atoms changed. We note that all of the three cases contribute to the local structural flexibility. The coordination of the atoms was determined using cutoff distances of 2.0, 3.0, and 2.0 Å for Z_{SiO} , Z_{NaO} , and Z_{BO} , respectively.

Figure 3 shows for the bulk glasses the percentage of coordination change p_α of species α with respect to its total number N_α as a function of strain. We consider here the sum of the three cases of coordination change as described before as an indicator of the intensity of local coordination change. For silica, one observes that p_{Si} only increases to around 3% at the strain of maximum strength, after which a sharp increase of p_{Si} is seen, which corresponds to its

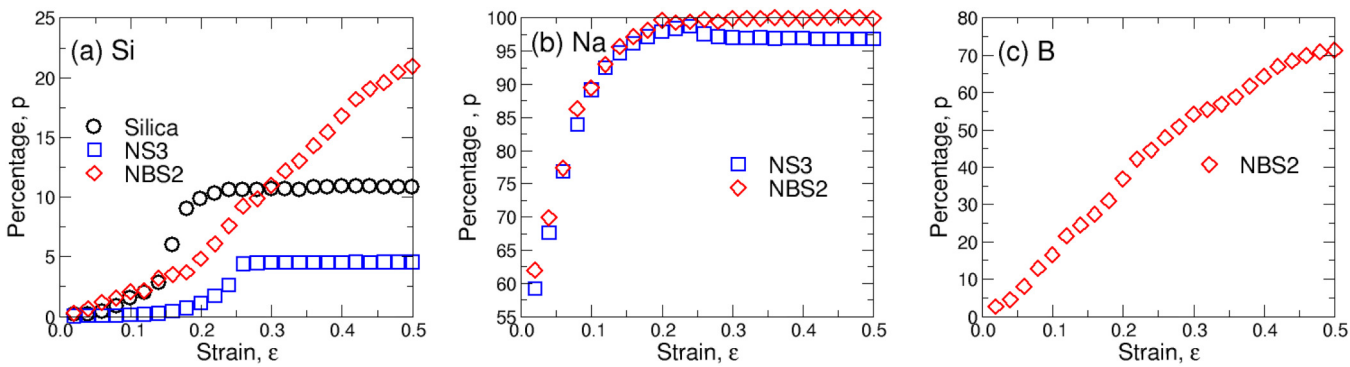


FIG. 3. Percentage of atoms that have changed their coordination during tension. See the main text for definition. (a)–(c) are for Si, Na, and B, respectively.

brittle fracture behavior. As the fracture is done and the stresses are released, the coordination of the atoms no longer change and, hence, p_{Si} reaches a constant value of around 10% at large strains. In contrast, p_{Si} for NS3 is nearly zero up to $\epsilon = 0.2$, indicating that Si coordination in NS3 is more stable and well preserved before failure. At $\epsilon > 0.2$, a notable increase in p_{Si} corresponds to mechanical failure of the glass. The strain-dependence of p_{Si} in NBS2 is different from silica and NS3 in that it constantly increases with strain and reaches about 20% at $\epsilon = 0.5$, considerably larger than that of silica and NS3. Boron in NBS2 exhibits an even stronger dependence on strain with over 70% of them changed coordination at $\epsilon = 0.5$.

In addition to the coordination change of the network formers, the flexibility imparted by the coordination change of the modifiers, i.e., Na, is also important. Figure 3(b) shows that Na is extremely active in changing its local coordination: For both NS3 and NBS2, only 20% of strain changes completely the coordination of the modifiers. This result is consistent with previous studies, which have shown that the network modifiers introduce plastic deformability to the structure by intensive bond switching during mechanical loading.^{38,54} Altogether, the coordination analysis indicates that the NBS2 glass benefits from the presence of mobile Na and structurally more flexible B compared to Si, enabling it to sustain larger deformation.

B. Response of the glasses under nanoindentation

After understanding the bulk glass properties, we now move on to discussing the properties of the three glasses under nanoindentation. It is worth noting that the max loading depth, 25 nm, would correspond to an intermediate strain (e.g., $10\% < \epsilon < 15\%$) as cracking appears in silica but not in NS3 or NBS2 (see below). This suggests that up to the probed indentation depth, both elasticity and plasticity contribute to the glass's mechanical response, with plasticity becoming more dominant as strain increases.

Figure 4 shows the macroscopic indentation response of the glass in terms of the force-displacement curve in Fig. 4(a) and the post-indentation height profiles in Fig. 4(b). The drop in force at the maximum indentation depth can be ascribed to stress relaxation during the holding stage. One observes that the force-displacement of silica is the highest, which can be attributed to the high rigidity of the fully polymerized Si-O network (see Table I). In contrast, although NBS2 also has a connected network structure, its rigidity is weakened by the mixed coordination of B and the mobile Na modifiers. The force-displacement curve of the NS3 glass is the lowest, as its highly depolymerized structure makes it softer and easier to penetrate. The depth of the indent remained after unloading is determined by the material's ability to sustain permanent deformation, which follows the order NBS2 > NS3 > silica, as seen from the stress-strain behavior in Fig. 2. Figure 4(b) shows that NBS2 has the largest pileup volume, while silica has the smallest. This is expected, as this property mainly depends on C_g : more densely packed glasses are less prone to densification and, thus, the volume is extruded as the indenter penetrates the glass. We also note that two regions with distinct slopes in the elevated volume above the contact surface, as reported in experiments,²⁵ were not observed in our simulations. This could be due to the relatively small sample size and indentation depth probed in our MD simulations.

Next, we discuss the changes in various atomic-level properties of the glasses in response to nanoindentation. The atomic stresses were calculated using the per-atom stress tensor formulation.⁵⁵ The atomic shear strain introduced by Shimizu *et al.*⁵⁶ was used to quantify local inelastic deformation. Densification was measured as the percentage density change relative to the density of the undeformed glass.

Figure 5 shows the maps of the local shear and normal stress components near the indent. At the largest loading depth, the maximum shear and normal stresses are estimated to be around 10 and 20 GPa, respectively, compatible with the estimation from

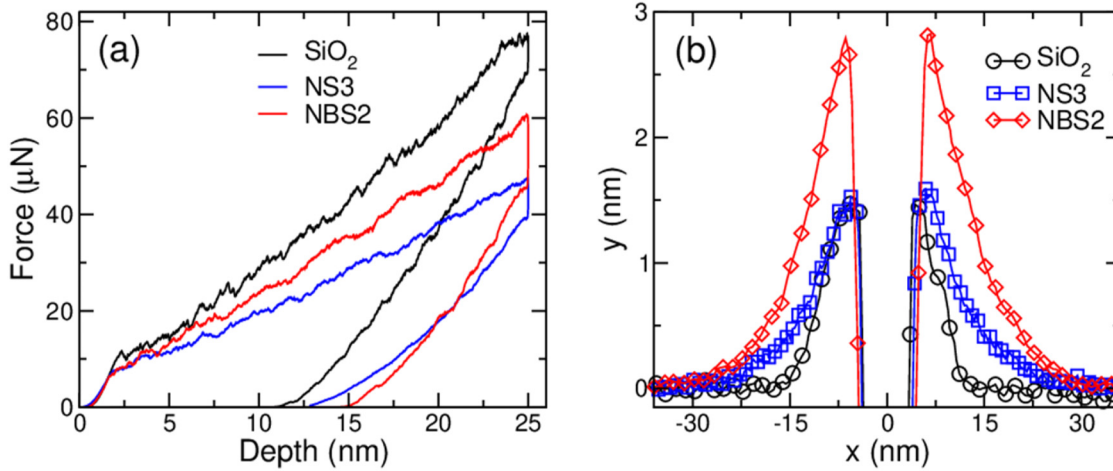


FIG. 4. (a) Force–displacement curve for the three glasses during the nanoindentation test. (b) Averaged y profile of the post-indentation glasses. Error bars are smaller than the symbol size.

24 December 2024 00:39:22

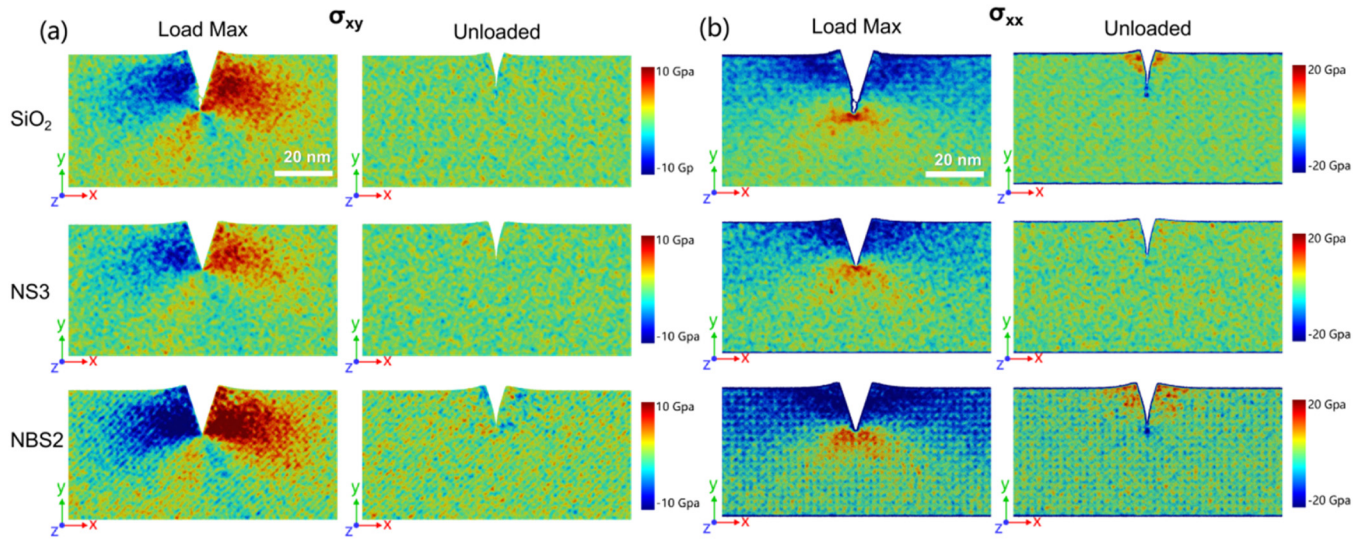


FIG. 5. Maps of (a) the shear stress σ_{xy} and (b) the normal stress σ_{xx} components for the three glasses at the maximum loading depth (load max) and after unloading (unloaded).

elasticity theories.⁵⁷ First, one recognizes that NS3 has the lowest stress level at the maximum loading depth, in accordance with its status as the softest of the three glasses (see Table I and Fig. 2). After unloading, stresses in NS3 are relaxed away due to the presence of modifiers that promote stress relaxation. In contrast, residual stresses, particularly the normal stress component σ_{xx} , persist in the pileup region of the unloaded silica and NBS2 samples. For silica, this stress is sufficiently high to induce cracking, as shown in

the snapshots at the maximum loading depth. Later, we will discuss how this residual stress can be attributed to the relatively high extent of permanent structural transformation (Fig. 9) in the two glasses, which places additional stress on the atomic bonds in the near-indent volume.

Figure 6 presents the maps of shear strain and densification for the three glasses after unloading. First, a small crack is visible in the silica glass but in NS3 and NBS2, indicating that silica is highly

24 December 2024 00:39:22

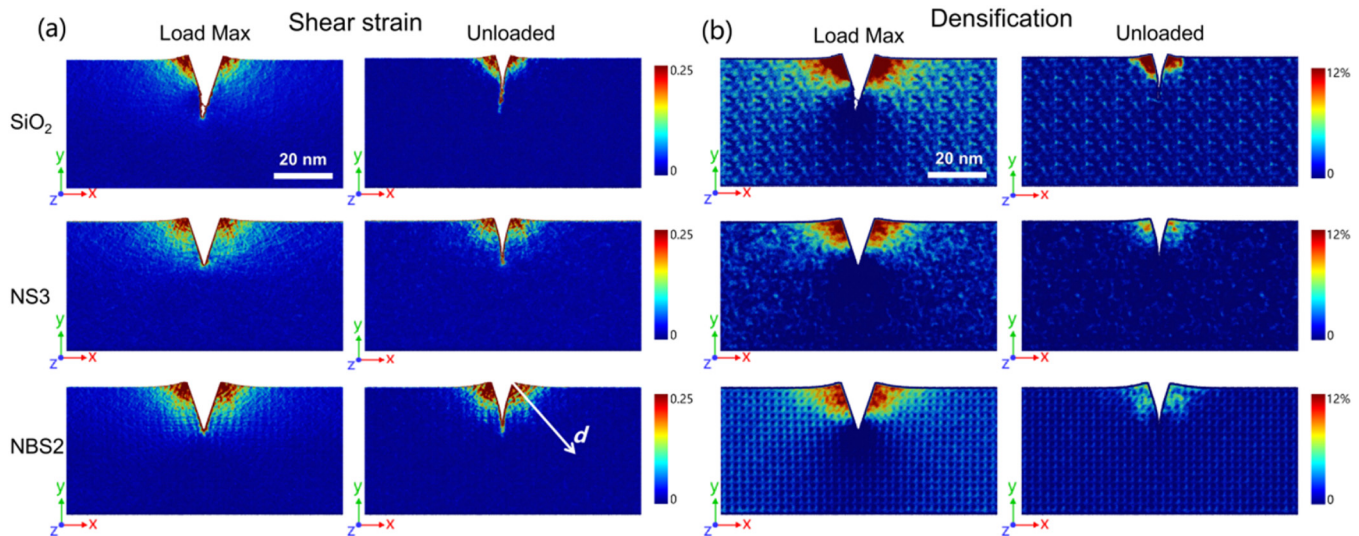


FIG. 6. Maps of (a) shear strain and (b) densification for the three glasses at the maximum loading depth (load max) and after unloading (unloaded).

susceptible to cracking, in accordance with its stress-strain behavior under uniaxial loading (Fig. 2). The lack of cracking in NBS2, despite considerable residual stress post-indentation, can be attributed to the high proportion of three-coordinated B (approximately 50% of B in the bulk NBS2 glass), which dissipate energy through structural transformation to tetrahedral coordination, thereby increasing resistance to residual stress-induced cracking.⁵⁷ Additionally, shear strain is more dispersed in NS3 and NBS2 than in silica, consistent with the finding that the former two glasses are structurally more flexible and can, therefore, activate plastic deformation more easily. After removing the indenter, residual strains can still be observed in all glasses, as they have all undergone permanent deformation to some extent. Figure 6(b) illustrates that densification is most pronounced in silica, which can be attributed to its high structural porosity (low C_g). In contrast, NS3 and NBS2 are more densely packed and structurally more flexible. Therefore, shear flow becomes the primary deformation mechanism in these glasses, resulting in minor marks of densification after unloading. Thus, one concludes that the ability of the glass to densify under indentation primarily depends on the atomic packing density of its structure.³ Furthermore, our results indicate that densification plays a primary role in inducing indentation cracking, contrasting with the conclusion of a recent study using a constitutive model, which suggests that shear flow is the predominant factor governing crack initiation in silicate glasses under indentation.⁵

To gain a clearer understanding of the deformation mechanisms of the glasses under indentation, we examined how the various atomic-level properties change from the pileup tip to the far-field regions, following the approach used in our previous study.²⁵ Specifically, the glass was sectioned into slices of thickness Δd , perpendicular to the specified direction [indicated by the arrow in Fig. 6(a)], forming a 45° angle with the negative y axis. We note that varying this partitioning angle by ±15° does not significantly affect the d -dependence of the distribution or the decay of these local properties.

Figure 7 shows the distribution of shear strain and densification as a function of distance d from the pileup tip. The shear strain near the indent is very broad (i.e., highly inhomogeneous), which gradually becomes narrower and shifts to smaller values as d increases, consistent with the snapshots in Fig. 5(a). Likewise, densification gradually decays when moving away from the indent, shown by the shift of the distribution profiles to smaller values.

To quantify the decay behavior of the two properties, Fig. 8 presents the mean values of shear strain and densification as a function of d . Shear strain [Fig. 8(a)], decays exponentially, independent of the composition. This kind of exponential decay has also been observed for other properties of oxide glasses such as the pair correlation function⁵⁸ and the height autocorrelation function of glass surfaces.⁵⁹ Fitting the data using the functional form $y \sim \exp(-d/\xi)$, where y denotes the mean value of the probed

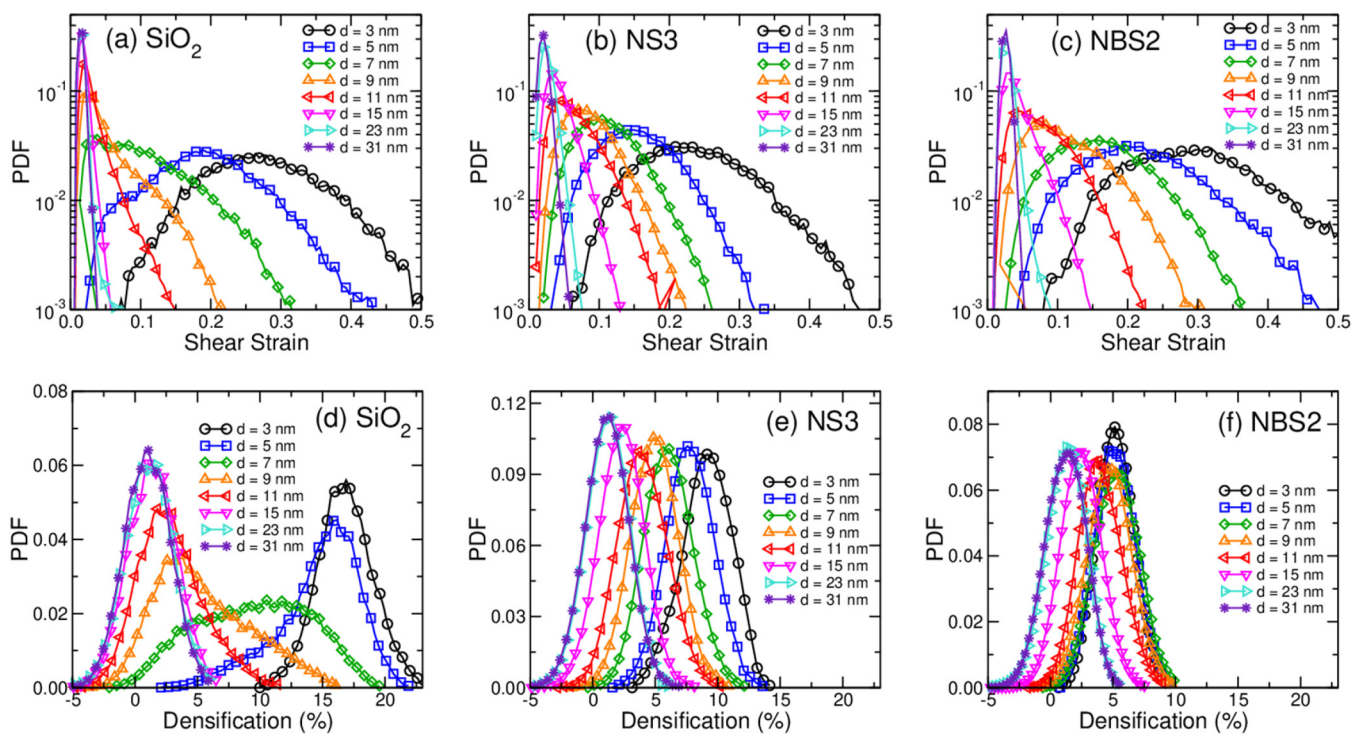


FIG. 7. Probability density function (PDF) of (a)–(c) shear strain and (d)–(f) densification in different regions ($\Delta d = 2$ nm) of the three glasses.

24 December 2024 00:39:22

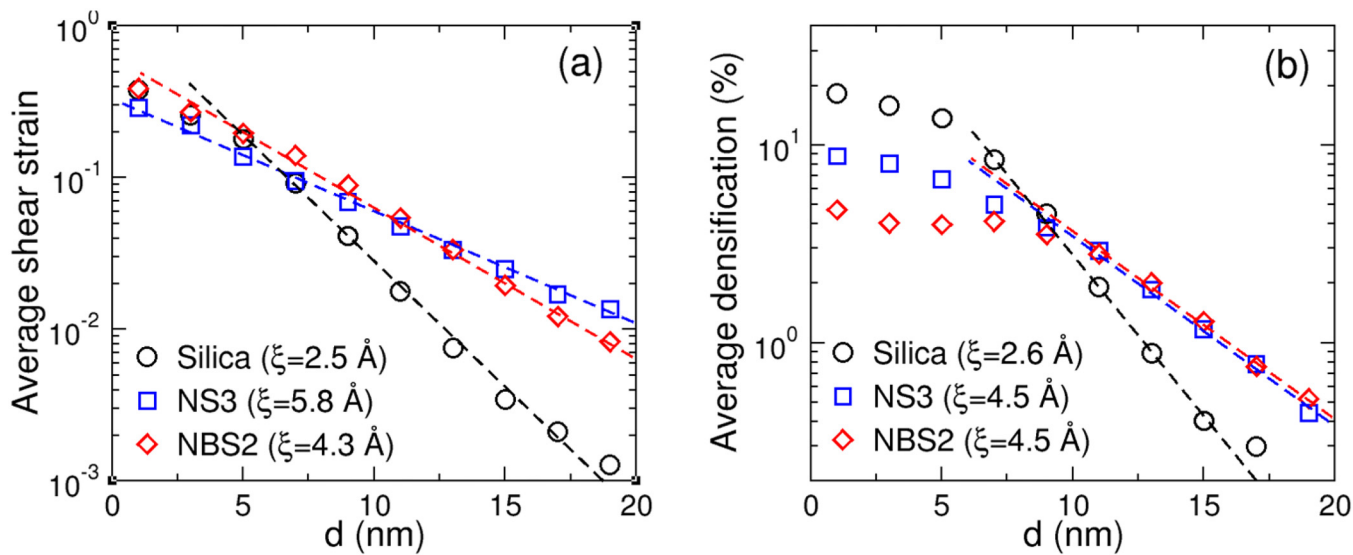


FIG. 8. Mean values of (a) shear strain and (b) densification in different regions ($\Delta d = 2 \text{ nm}$) of the three glasses. Error bars are smaller than the symbol size. Dashed lines are exponential fits to the data sets.

property, allows one to estimate the decay length ξ . Usually, 3ξ can be considered the typical correlation length of the probed property. One observes that shear strain in silica decays fastest with $\xi = 2.5 \text{ \AA}$, indicating that plastic deformation in silica is most concentrated around the indent, in accordance with its rigid network structure. In contrast, the decay lengths for NBS2 and NS3 are considerably larger, with NS3 decaying the slowest, likely due to its more depolymerized network compared to NBS2 (see Table I).

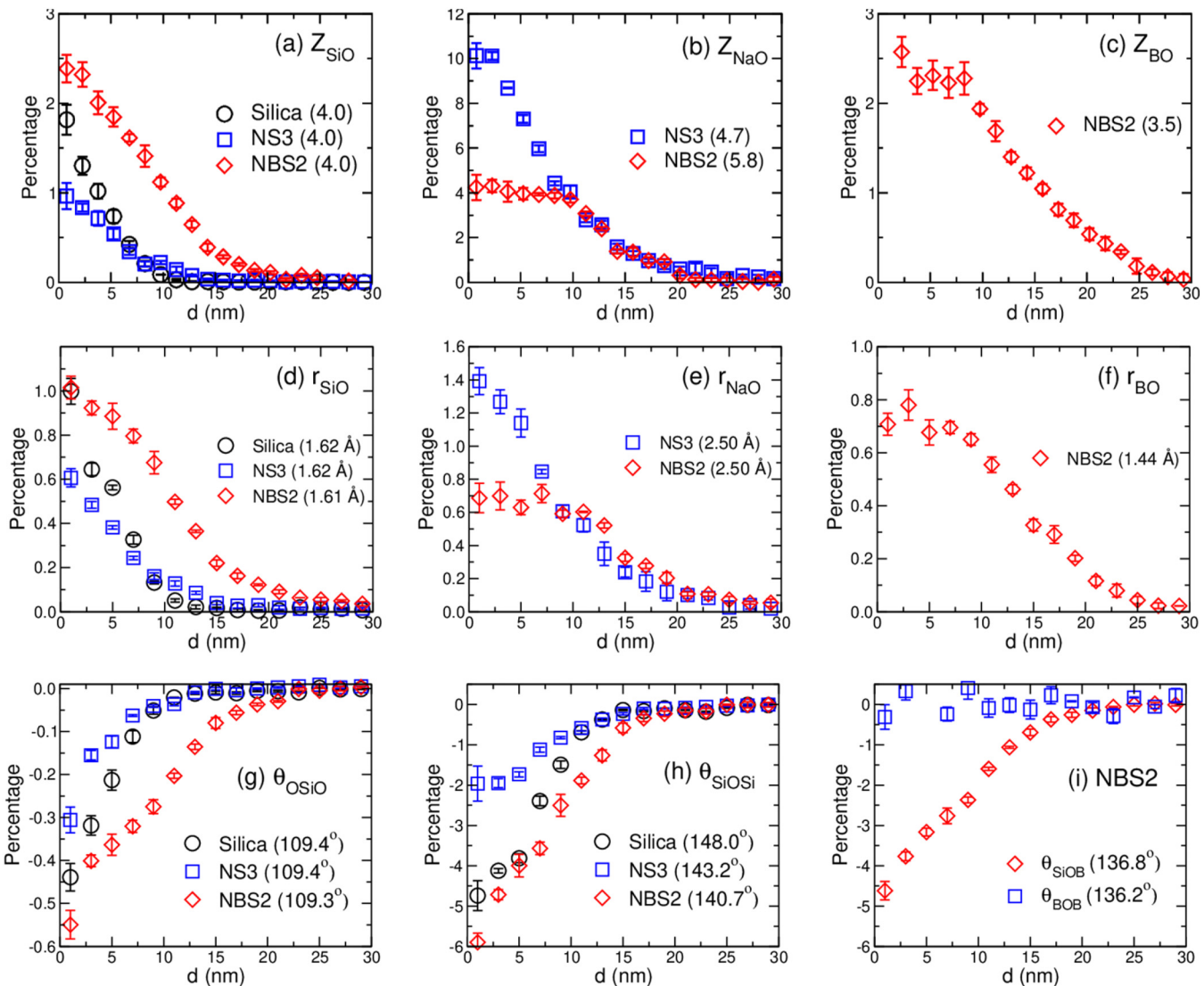
Figure 8(b) shows that the decay behavior of densification is more complex since it is d -dependent. Specifically, densification decreases relatively slowly at small d , with the rate depending on the composition. This result can be rationalized by the high ratio between effective volumetric yield stress (due to increased atomic repulsion) and flow stress (which triggers shear flow) in the near-tip region, causing densification to reach saturation and that deformation is directed by shear flow. The degree of densification in the near-indent region follows the order NBS2 > NS3 > silica, which can be attributed to the different C_g of the glasses. As d increases, a crossover in the d -dependence occurs at $d \approx 8 \text{ nm}$, beyond which data for all glasses fit an exponential function, allowing for estimating the decay length for densification. First, the decay lengths for densification are comparable to those for shear strain, consistent with earlier studies showing that densification is assisted by concomitant shear stresses in glasses prone to density increase.⁵⁰ Additionally, densification decays fastest in silica with $\xi = 2.6 \text{ \AA}$, while NS3 and NBS2 decay much slower with a $\xi=4.5 \text{ \AA}$. This contrasts the shear strain decay behavior in these glasses, indicating that Na modifiers play a more decisive role than network connectivity in governing the decay of densification.

To better understand the deformation behavior of the glasses, it is important to examine the structural features on short-to-intermediate length scales. First, we discuss the variation

in short-range structural order (SRO) induced by indentation. Figures 9(a)–9(c) illustrate the change in the coordination number (Z) of cations after indentation. For a clearer comparison of the decay behavior, the three panels show the percentage change of the mean coordination number with respect to the bulk value, i.e., $(Z_{\alpha\beta}(d) - Z_{\alpha\beta}^{\text{bulk}})/Z_{\alpha\beta}^{\text{bulk}} \times 100$, where $Z_{\alpha\beta}(d)$ denotes the mean number of β atoms in the nearest neighbor of an α atom at distance d , and $Z_{\alpha\beta}^{\text{bulk}}$ is the corresponding value for the bulk glass (in parentheses).

Figure 9(a) shows that at small d , the change of Z_{SiO} in NBS2 and silica is more pronounced compared to NS3, indicating stronger permanent densification in the former two glasses, consistent with the snapshots in Fig. 6(b). The pronounced change of Z_{SiO} in NBS2 can be attributed to the addition of B_2O_3 , which not only makes the network more flexible but also increases the O/Si ratio. Both factors enable Si atoms to more easily change their coordination under indentation compared to silica and NS3.

Figure 9(b) shows that the coordination change of Na in NBS2 remains nearly constant at short-to-intermediate d , indicating that the structural transformation in terms of the Na coordination is saturated in this region, likely due to the high packing density of NBS2. In contrast, Na coordination in NS3 shows a more gradual, exponential-like decay, due to its lower packing density and more depolymerized structure. The coordination of B in NBS2 also exhibits a plateau, similar to Na, at short-to-intermediate d . This suggests that the structural transition of B from three-coordinated to four-coordinated occurs relatively easily, leading to saturation in B coordination change. A similar d -dependence is also observed for cation–oxygen bond lengths, Figs. 9(d)–(f), although the magnitudes of the changes are significantly smaller than those of coordination numbers, due to the high strength and rigidity of the bonds.



24 December 2024 00:39:22

FIG. 9. Percentage change of various short-range structural quantities relative to the bulk values (given in parenthesis) as a function of distance d from the pileup tip. (a)–(c) Coordination numbers, (d)–(f) bond lengths, (g)–(i) bond angles.

The change in the O-Si-O angle with d is minimal, which can be attributed to the high energy required to deform $[\text{SiO}_4]$ tetrahedral units. In contrast, bending the linkages between these structural units, i.e., Si-O-Si/B angles, is easier [see Figs. 9(h) and (i)]. The change in the Si-O-Si angle follows the order NBS2 > SiO_2 > NS3, which may result from the competition between network rigidity and atomic packing density. Specifically, NS3's structure is relatively flexible due to high depolymerization and moderate packing density, which makes structural compaction via tetrahedral unit rotation energetically favorable, without significant changes to inter-tetrahedral angles. In contrast,

NBS2 has both a rigid network (comparable to that of NS3) and a dense atomic packing. This makes rotational motion of the structural units difficult due to steric constraints, and, hence, deformation involves larger angular changes. Silica, unlike the other two glasses, has a highly polymerized network but a low packing density. The balance between these factors results in an intermediate level of inter-tetrahedral angular changes. One also recognizes that, in the highly cross-linked NBS2 glass, the B-O-B linkages are much more stiff than the Si-O-Si and Si-O-B connections, so that the B-O-B angle barely changes with d [see panel (i)].

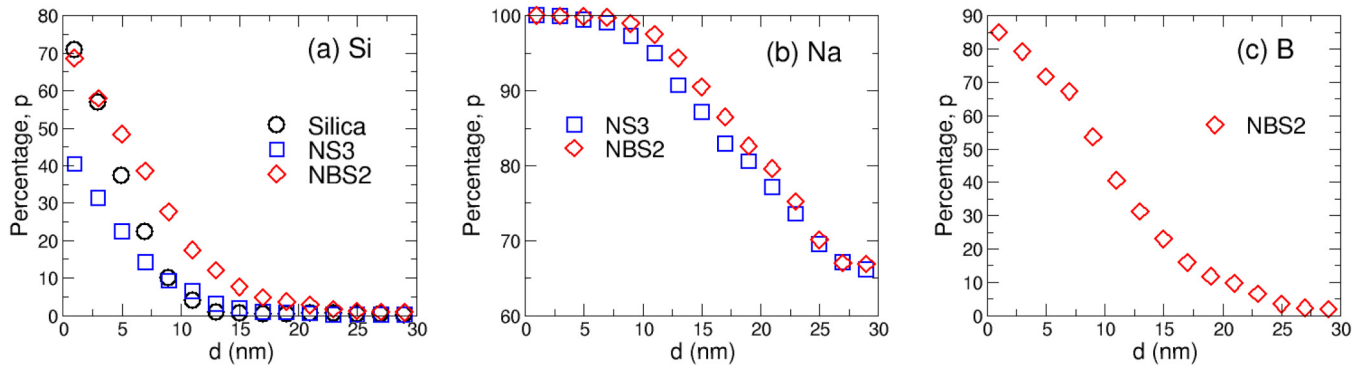


FIG. 10. Percentage of atoms that have changed their coordination after indentation. See the main text for definition. (a)–(c) are for Si, Na, and B, respectively. $\Delta d = 2$ nm.

Notably, most of the SRO quantities exhibit an exponential-like decay at intermediate-to-large d , consistent with the behavior of shear strain and densification (see Fig. 8). These results indicate a close relationship between local structural changes and the mechanical response of glasses under a sharp contact load.

Furthermore, we have performed bond switching analysis for the glasses after indentation. Figure 10 shows the percentages of the various atomic species that have changed their coordination as a function of distance d from the pileup tip. One observes that 100% of Na and more than 85% of B in the vicinity of the pileup have changed their coordination when compared to the undeformed state. In contrast, p_{Si} is lower than p_{Na} and p_B and exhibits a composition-dependence that is consistent with the results for the bulk glasses (see Fig. 3). With increasing d , the decay of p_{Si} is the fastest, followed by p_B and p_{Na} . We note that the coordination of

Na changes with deformation as well as time (due to its high mobility), which explains the fact that even at $d = 30$ nm (where p_{Si} and p_B have decreased to zero), still over 60% of Na have changed their coordination after unloading. To summarize, these results indicate that the structure right below the indent is highly modified and that the flexibility of the local environment of the atomic species follows the order Na > B > Si.

Figure 11 shows the spatial distribution of the atoms that have increased Z at the maximum loading depth (max load) and after unloading (unloaded), with respect to the initial undeformed state. The atoms are colored based on their local number density. One observes that the coordination change of Si is mostly concentrated in the pileup region. In contrast, the distribution of B with changed coordination is more spread out, indicating the B local structure is softer than that around Si. Furthermore, one observes that Na with

24 December 2024 00:39:22

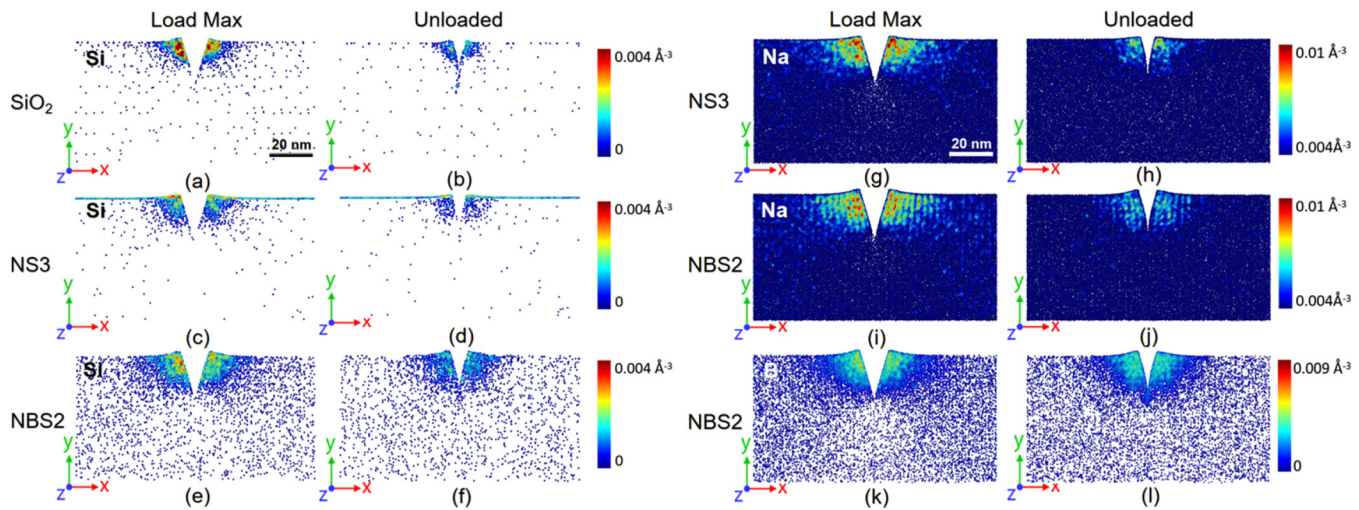
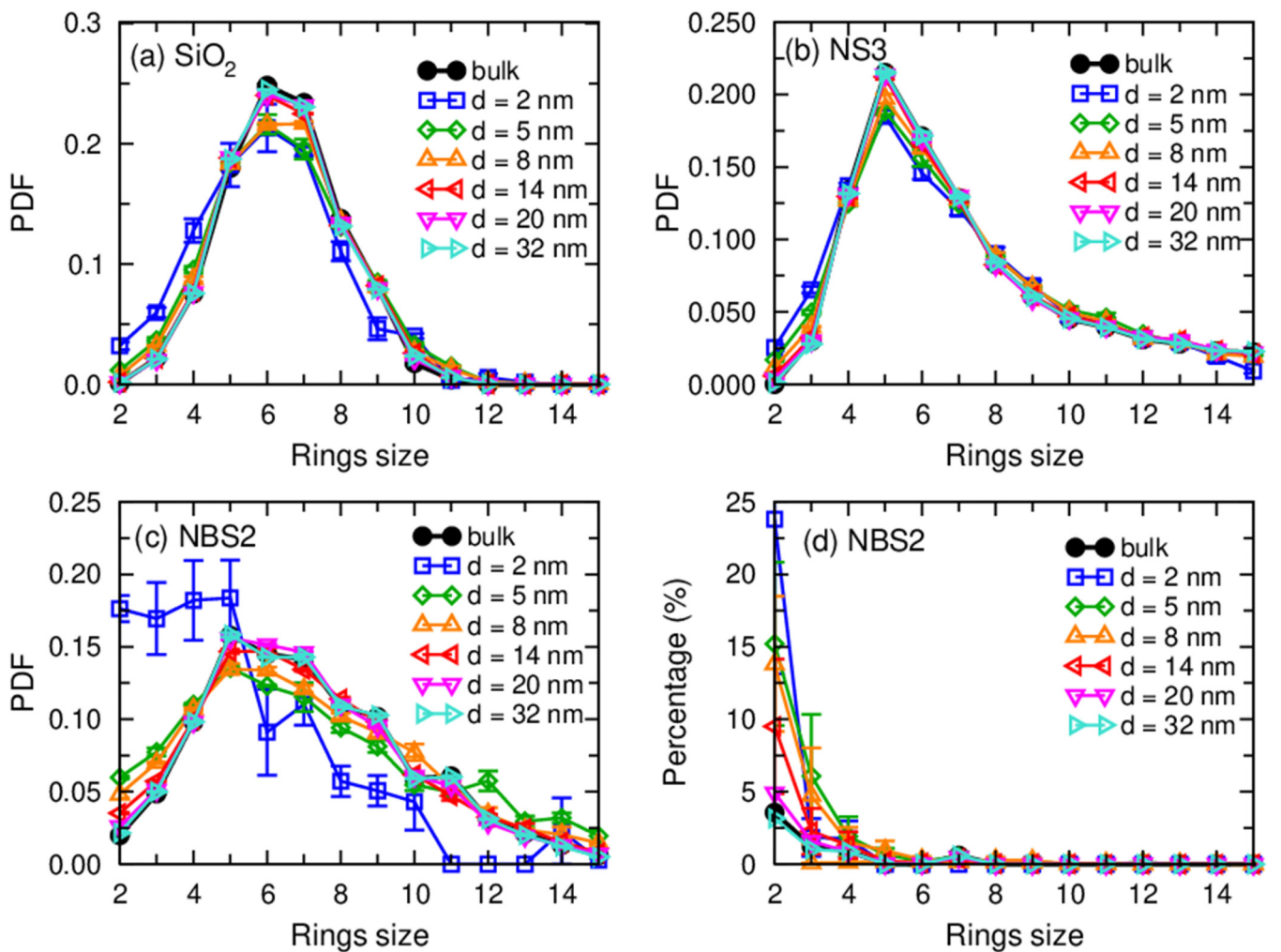


FIG. 11. Spatial distribution of the atoms that have increased their coordination number at the maximum loading depth (load max) and after unloading (unloaded), with respect to the initial undeformed state. (a)–(f) Si. (g)–(j) Na. (k)–(l) B.

changed coordination distributes almost all over the sample, with a notably higher density in the near-tip region, consistent with the fact that Na is the most mobile species and that a large fraction of Na has changed their coordination during indentation deformation.

From Fig. 11, one can infer another interesting structural property of the glasses, i.e., reversibility of local coordination, which has been shown to be important for the damage resistance of oxide glasses.¹¹ We note that here we do not consider the cases that the atoms have decreased Z (which is very rare) and Z unchanged but neighbor changed to allow fair comparison with the literature. However, we note that if the two cases are taken into account, in particular the atoms with Z unchanged but neighbor changed, almost all atoms will be classified as non-recoverable. Based on the population of atoms with increased Z at the maximum loading depth and after unloading, we find that the recovery ratio for Si is 73%, 41%, and

42% for silica, NS3, and NBS2, respectively. The corresponding ratio for Na is 13%, independent of composition. The recovery ratio for B is 16%, slightly higher than Na but considerably lower than Si. A recent simulation study by Liu *et al.*¹¹ found that more B atoms experience reversible coordination change than Si atoms in multi-component oxide glasses during indentation, which seems to contradict our results. However, if one consider the *fraction* of atoms (instead of the number of atoms, which is system size- and composition-dependent) that have experienced this coordination conversion, we find that also their data suggest that Si is *more* reversible than B, thus in line with our finding. The rationale for the larger reversibility of Si than B might be that the fivefold coordinated Si, which forms under compression is only metastable, i.e., it tends to convert to a more stable local fourfold coordinated configuration upon stress relaxation. In contrast, both three- and



24 December 2024 00:39:22

FIG. 12. Ring size distribution in different regions of the three glasses after indentation. (a) SiO_2 , (b) NS3, (c) and (d) NBS2. (d) Fraction of rings containing only Si and O nodes.

fourfold coordinated B coexist in the pristine glass and are relatively stable. Hence, once the coordination is transformed from one state to another, it is difficult to get recovered since this process requires to overcome a high energy barrier.

Beyond short-range structures, structural features on larger length scales, in particular the medium-range structural order (MRO), also change as the indenter is penetrated into the glass. Figure 12 shows the change in the MRO in terms of the ring structures (i.e., closed loop of Si-O and/or B-O bonds), determined using the primitive ring criterion.⁶¹ For comparison, the panels also include data for the bulk glasses. First, one observes that the most probable ring size (n) in silica is six, regardless of the distance from the indent. In contrast, the most probable ring size for NS3 and NBS2 is five. In addition to the difference in the most probable ring size, NS3 and NBS2 have a broader ring size distribution than silica. This suggests that greater chemical complexity induces more structural heterogeneity at medium-range length scales, consistent with previous studies.^{34,62}

In silica, the near-tip region ($d = 2$ nm), where severe deformation has occurred, shows significantly lower probabilities of intermediate-to-large-sized rings ($5 \leq n \leq 9$) compared to larger distances and the bulk value. In contrast, the fractions of small-sized rings ($2 \leq n \leq 4$) are notably higher, indicating a pronounced transformation in the network topology. This structural change decays rapidly, and by $d \approx 10$ nm, the ring size distribution converges toward the bulk distribution. In NS3, the d -dependence of the ring size distribution is slightly weaker but qualitatively similar to silica. This aligns with the finding that local properties decay more slowly (i.e., with a larger decay length) in NS3. In NBS2, a significant MRO transformation occurs in the pileup region, where most rings have converged to small-sized ones. This can be attributed to NBS2's highly cross-linked yet relatively flexible network, which is prone to severe permanent structural transformation under compression. This change in NBS2's network topology persists over larger distances than in silica and NS3, consistent with the decay behavior of the SRO quantities (Fig. 9). This indicates that the evolution of the SRO and MRO are strongly correlated under a sharp contact loading.

Compared to silica and NS3, the complexity in the structure of NBS2 arises from the fact that its ring structures may contain both Si and B nodes. Further insight into the indentation-induced changes in MRO can be gained by decomposing the rings into pure Si-O rings and Si-B mixed rings. Figure 12(d) shows the fraction of pure Si-O rings by size and their dependence on d . In the bulk glass, only about 7% of two-membered (2 M) rings (formed by two polyhedra sharing an edge) are formed by pure Si-O bonds, while almost all larger rings are a mixture of Si and B. This highlights the highly cross-linked nature of the NBS2's network structure. Interestingly, in the severely deformed region near the pileup tip, about 25% of the 2 M rings are pure Si-O rings. Considering the high fraction of 2 M rings, the density of pure Si-O 2 M rings in this region is much higher than in the bulk glass. This suggests that the decomposition of medium-to-large rings into smaller ones, especially 2 M rings, is accompanied by elemental redistribution, potentially resulting in Si- or B-rich micro-domains. As d increases, the compositional and structural inhomogeneities decrease and at $d > 20$ nm, the bulk properties are largely restored.

IV. SUMMARY AND CONCLUSIONS

Using large-scale MD simulations, we have studied the indentation response of three prototypical silicate glasses with varying compositional complexity. The primary goal has been to understand how the network modifier Na and the secondary network former B influence the response of silicate glasses under highly localized stress induced by a sharp indenter.

The distinct mechanical responses of the glasses are linked to structural features like bonding type/strength, network connectivity, and atomic packing density. Specifically, the differences in the elastic properties of the three bulk glasses can be explained by their different bond strength density, which depends on both bonding type and bond density. In contrast, the greater nano-ductility exhibited by the NS3 and NBS2 glasses relative to silica is due to the structural flexibility provided by the network-modifying Na and the B species with mixed coordination, which is evidenced from the pronounced bond switching activities of these two species as compared to Si.

Shear flow is found to be more pronounced in NS3 and NBS2, while densification is more prominent in silica, indicating that the former deformation mode is more easily activated in systems with high structural flexibility, whereas the latter mode depends on the structure's packing density. Additionally, we find that the decay of shear strain mainly depends on network connectivity (i.e., more depolymerized structure decays more slowly), while the decay of densification is primarily influenced by the concentration of network modifiers.

Changes in the Si-O network features follow the order: NBS2 > silica > NS3, due to the competition between network rigidity and atomic packing density. B-O-B linkages are significantly stiffer than the Si-O-Si and Si-O-B connections, resulting in minimal changes to the B-O-B angle beneath the indent. On intermediate-range length scales, the transformation of network topology, particularly in ring structures, is most pronounced in NBS2, with a large fraction of small-sized rings forming near the indent, possibly involving the formation of nanometer-sized domains enriched in B or Si. Structural changes at short-to-intermediate length scales are closely correlated and are the structural origin of the distinct mechanical response of the glasses under nanoindentation. These microscopic insights will be useful for the rational design of damage-resistant glassy materials by optimizing glass composition.

ACKNOWLEDGMENTS

The authors gratefully acknowledge financial support from the National Natural Science Foundation of China (NNSFC) (Nos. U22A20125, 52102002, U24A2052, and 12474185), Shanghai Municipal Natural Science Foundation (No. 22ZR1400400), Shanghai Pujiang Program (No. 22PJD002), and the Fundamental Research Funds for the Central Universities (No. 2232024G-07).

AUTHOR DECLARATIONS

Conflict of Interest

The authors have no conflicts to disclose.

24 December 2024 00:39:22

Author Contributions

Z.Y. and R.L. contributed equally to this paper.

Ziming Yan: Conceptualization (equal); Data curation (equal); Formal analysis (equal); Investigation (equal); Methodology (equal); Resources (equal); Supervision (equal); Visualization (equal); Writing – original draft (equal); Writing – review & editing (equal). **Ranran Lu:** Data curation (equal); Formal analysis (equal); Investigation (equal); Visualization (equal); Writing – original draft (equal). **Linfeng Ding:** Conceptualization (equal); Data curation (equal); Formal analysis (equal); Funding acquisition (equal); Investigation (equal); Resources (equal); Writing – original draft (equal). **Lianjun Wang:** Conceptualization (equal); Funding acquisition (equal); Resources (equal); Writing – original draft (equal). **Zhen Zhang:** Conceptualization (equal); Funding acquisition (equal); Methodology (equal); Resources (equal); Supervision (equal); Writing – review & editing (equal).

DATA AVAILABILITY

The data that support the findings of this study are available from the corresponding authors upon reasonable request.

REFERENCES

- ¹A. K. Varshneya and J. C. Mauro, *Fundamentals of Inorganic Glasses*, 3rd ed. (Elsevier, Amsterdam, 2019).
- ²L. Wondraczek, E. Bouchbinder, A. Ehrlicher, J. C. Mauro, R. Sajzew, and M. M. Smedskjaer, “Advancing the mechanical performance of glasses: Perspectives and challenges,” *Adv. Mater.* **34**(14), e2109029 (2022).
- ³T. Rouxel, J. I. Jang, and U. Ramamurty, “Indentation of glasses,” *Prog. Mater. Sci.* **121**(4), 2625 (2021).
- ⁴M. Kazembeyki, K. Yang, J. C. Mauro, M. M. Smedskjaer, M. Bauchy, and C. G. Hoover, “Decoupling of indentation modulus and hardness in silicate glasses: Evidence of a shear-to densification-dominated transition,” *J. Non-Cryst. Solids* **553**(11), 2203 (2021).
- ⁵E. Barthel, V. Kervyn, G. Rosales-Sosa, and G. Kermouche, “Indentation cracking in silicate glasses is directed by shear flow, not by densification,” *Acta Mater.* **194**(11), 473 (2020).
- ⁶K. W. Peter, “Densification and flow phenomena of glass in indentation experiments,” *J. Non-Cryst. Solids* **5**(2), 103 (1970).
- ⁷D. A. Kilymisi and J. M. Delaye, “Deformation mechanisms during nanoindentation of sodium borosilicate glasses of nuclear interest,” *J. Chem. Phys.* **141**(1), 014504 (2014).
- ⁸D. A. Kilymisi, J. M. Delaye, and S. Ispas, “Nanoindentation of the pristine and irradiated forms of a sodium borosilicate glass: Insights from molecular dynamics simulations,” *J. Chem. Phys.* **145**(4), 044505 (2016).
- ⁹J. Kjeldsen, M. M. Smedskjaer, J. C. Mauro, and Y. Yue, “Hardness and incipient plasticity in silicate glasses: Origin of the mixed modifier effect,” *Appl. Phys. Lett.* **104**(5), 486 (2014).
- ¹⁰D. H. Lee, I. C. Choi, M. Y. Seok, Y. Zhao, J. A. Lee, J. i. Jang, and T. Rouxel, “Strain-dependent plasticity evolution of window glass,” *J. Am. Ceram. Soc.* **98**(1), 186 (2015).
- ¹¹H. Liu, B. Deng, S. Sundararaman, Y. Shi, and L. Huang, “Understanding the response of aluminosilicate and aluminoborate glasses to sharp contact loading using molecular dynamics simulation,” *J. Appl. Phys.* **128**(3), 035106 (2020).
- ¹²J. Luo, K. D. Vargheese, A. Tandia, G. Hu, and J. C. Mauro, “Crack nucleation criterion and its application to impact indentation in glasses,” *Sci. Rep.* **6**(2), 23720 (2016).
- ¹³E. Moayedi, S. Sawamura, J. Hennig, E. Gnecco, and L. Wondraczek, “Relaxation of scratch-induced surface deformation in silicate glasses: Role of densification and shear flow in lateral indentation experiments,” *J. Non-Cryst. Solids* **500**(36), 382 (2018).
- ¹⁴K. I. Nomura, Y. C. Chen, R. K. Kalia, A. Nakano, and P. Vashishta, “Defect migration and recombination in nanoindentation of silica glass,” *Appl. Phys. Lett.* **99**(11), 382 (2011).
- ¹⁵T. Rouxel, H. Ji, T. Hammouda, and A. Moréac, “Poisson’s ratio and the densification of glass under high pressure,” *Phys. Rev. Lett.* **100**(22), 225501 (2008).
- ¹⁶P. Sellappan, T. Rouxel, F. Celarie, E. Becker, P. Houizot, and R. Conradt, “Composition dependence of indentation deformation and indentation cracking in glass,” *Acta Mater.* **61**(16), 5949 (2013).
- ¹⁷S. Striepe, J. Deubener, M. Potuzak, M. M. Smedskjaer, and A. Matthias, “Thermal history dependence of indentation induced densification in an aluminosilicate glass,” *J. Non-Cryst. Solids* **445**(11), 34 (2016).
- ¹⁸Z. Wan, W. Wang, J. Feng, L. Dong, S. Yang, and Z. Jiang, “Effect of scratch direction on densification and crack initiation of optical glass BK7,” *Ceram. Int.* **46**(10), 16754 (2020).
- ¹⁹S. Yoshida, J. C. Sangleboeuf, and T. Rouxel, “Quantitative evaluation of indentation-induced densification in glass,” *J. Mater. Res.* **20**(12), 3404 (2005).
- ²⁰C. Zehnder, J. N. Peltzer, J. S. K. Gibson, D. Möncke, and S. Korte-Kerzel, “Non-Newtonian flow to the theoretical strength of glasses via impact nanoindentation at room temperature,” *Sci. Rep.* **7**(1), 17618 (2017).
- ²¹T. Rouxel, H. Ji, J. P. Guin, F. Augereau, and B. Rufflé, “Indentation deformation mechanism in glass: Densification versus shear flow,” *J. Appl. Phys.* **107**(9), 34 (2010).
- ²²K. Januchta and M. M. Smedskjaer, “Indentation deformation in oxide glasses: Quantification, structural changes, and relation to cracking,” *J. Non-Cryst. Solids* **X** **1**(2590), 100007 (2019).
- ²³T. M. Gross, J. Wu, D. E. Baker, J. J. Price, and R. Yongsunthon, “Crack-resistant glass with high shear band density,” *J. Non-Cryst. Solids* **494**, 13 (2018).
- ²⁴H. Duan, A. L. Ogrinc, Y. T. Lin, R. Hengstebeck, B. Dong, J. Yu, S. V. Rotkin, H. He, and S. H. Kim, “Quasistatic nature of subsurface densification of soda lime silicate glass under nano-and Vickers indentation,” *Ceram. Int.* **50**(18), 32457 (2024).
- ²⁵L. Ding, Y. Xu, R. Yang, Y. Yang, R. Lu, H. Liu, H. He, Q. Zheng, and J. C. Mauro, “Lateral-pushing induced surface lift-up during nanoindentation of silicate glass,” *J. Am. Ceram. Soc.* **105**(4), 2625 (2022).
- ²⁶D. A. Kilymisi and J. M. Delaye, “Nanoindentation of pristine and disordered silica: Molecular dynamics simulations,” *J. Non-Cryst. Solids* **382**(11), 87 (2013).
- ²⁷D. A. Kilymisi and J. M. Delaye, “Nanoindentation studies of simplified nuclear glasses using molecular dynamics,” *J. Non-Cryst. Solids* **401**(9), 147 (2014).
- ²⁸H. Liu, Y. Shi, and L. Huang, “Deformation behaviors of a model metallic glass under 3-D nanoindentation studied in molecular dynamics simulation,” *J. Non-Cryst. Solids X* **16**(7), 100130 (2022).
- ²⁹Y. Kato, H. Yamazaki, S. Yoshida, and J. Matsuoka, “Effect of densification on crack initiation under Vickers indentation test,” *J. Non-Cryst. Solids* **356**(35), 1768 (2010).
- ³⁰S. Yoshida, H. Sawasato, T. Sugawara, Y. Miura, and J. Matsuoka, “Effects of indenter geometry on indentation-induced densification of soda-lime glass,” *J. Mater. Res.* **25**(11), 2203 (2010).
- ³¹C. Hermansen, J. Matsuoka, S. Yoshida, H. Yamazaki, Y. Kato, and Y. Z. Yue, “Densification and plastic deformation under microindentation in silicate glasses and the relation to hardness and crack resistance,” *J. Non-Cryst. Solids* **364**(9), 40 (2013).
- ³²L. Ding, R. Lu, L. Wang, Q. Zheng, J. C. Mauro, and Z. Zhang, “Nanoindentation-induced evolution of atomic-level properties in silicate glass: Insights from molecular dynamics simulations,” *J. Am. Ceram. Soc.* **107**(3), 1448 (2024).
- ³³S. Sundararaman, L. Huang, S. Ispas, and W. Kob, “New interaction potentials for borate glasses with mixed network formers,” *J. Chem. Phys.* **152**(10), 104501 (2020).

- ³⁴S. Sundararaman, L. Huang, S. Ispas, and W. Kob, "New interaction potentials for alkali and alkaline-earth aluminosilicate glasses," *J. Chem. Phys.* **150**(15), 154505 (2019).
- ³⁵S. Sundararaman, L. Huang, S. Ispas, and W. Kob, "New optimization scheme to obtain interaction potentials for oxide glasses," *J. Chem. Phys.* **148**(19), 194504 (2018).
- ³⁶D. Wolf, P. Kebinski, S. R. Phillpot, and J. Eggebrecht, "Exact method for the simulation of coulombic systems by spherically truncated, pairwise r^{-1} summation," *J. Chem. Phys.* **110**(17), 8254 (1999).
- ³⁷Z. Zhang, S. Ispas, and W. Kob, "The critical role of the interaction potential and simulation protocol for the structural and mechanical properties of sodosilicate glasses," *J. Non-Cryst. Solids* **532**(1), 186 (2020).
- ³⁸Z. Zhang, S. Ispas, and W. Kob, "Origin of the non-linear elastic behavior of silicate glasses," *Acta Mater.* **231**(10), 16754 (2022).
- ³⁹Z. Zhang, S. Ispas, and W. Kob, "Fracture of silicate glasses: Microcavities and correlations between atomic-level properties," *Phys. Rev. Mater.* **6**(8), 16754 (2022).
- ⁴⁰Z. Zhang, S. Ispas, and W. Kob, "Roughness and scaling properties of oxide glass surfaces at the nanoscale," *Phys. Rev. Lett.* **126**(6), 066101 (2021).
- ⁴¹N. P. Bansal and R. H. Doremus, *Handbook of Glass Properties* (Elsevier, Amsterdam, 2013).
- ⁴²G. Scannell, S. Barra, and L. Huang, "Structure and properties of $\text{Na}_2\text{O}-\text{TiO}_2-\text{SiO}_2$ glasses: Role of Na and Ti on modifying the silica network," *J. Non-Cryst. Solids* **448**(9), 52 (2016).
- ⁴³A. K. Varshneya, *Fundamentals of Inorganic Glasses* (Elsevier, Amsterdam, 2013).
- ⁴⁴Z. Zhang, J. Ding, and E. Ma, "Shear transformations in metallic glasses without excessive and predefinable defects," *Proc. Natl. Acad. Sci. U.S.A.* **119**(48), e2213941119 (2022).
- ⁴⁵Y. Yang, J. Luo, L. Huang, G. Hu, K. D. Vargheese, Y. Shi, and J. C. Mauro, "Crack initiation in metallic glasses under nanoindentation," *Acta Mater.* **115**(9), 413 (2016).
- ⁴⁶X. Lu, L. Deng, J. Du, and J. D. Vienna, "Predicting boron coordination in multicomponent borate and borosilicate glasses using analytical models and machine learning," *J. Non-Cryst. Solids* **553**(17), 8254 (2021).
- ⁴⁷T. Nanba, M. Nishimura, and Y. Miura, "A theoretical interpretation of the chemical shift of ^{29}Si NMR peaks in alkali borosilicate glasses," *Geochim. Cosmochim. Acta* **68**(24), 5103 (2004).
- ⁴⁸A. A. Osipov, V. E. Eremyshev, and L. M. Osipova, "Structure of Ca-Sr-Ba sodium-borosilicate glasses according to ^{11}B and ^{29}Si NMR spectroscopy," *Glass Phys. Chem.* **44**(2), 71 (2018).
- ⁴⁹Y. H. Yun and P. J. Bray, "Nuclear magnetic resonance studies of the glasses in the system $\text{Na}_2\text{OB}_2\text{O}_5\text{SiO}_2$," *J. Non-Cryst. Solids* **27**(3), 363 (1978).
- ⁵⁰V. Dimitrov and T. Komatsu, "Polarizability, basicity and chemical bonding of single and multicomponent oxide glasses," *J. Chem. Technol. Metall.* **50**(4), 387 (2015).
- ⁵¹V. Dimitrov and T. Komatsu, "Relationship between optical basicity and average single bond strength of oxide glasses," *Phys. Chem. Glasses* **46**(5), 521 (2005).
- ⁵²G. N. Greaves, A. L. Greer, R. S. Lakes, and T. Rouxel, "Poisson's ratio and modern materials," *Nat. Mater.* **10**(11), 823 (2011).
- ⁵³B. Wang, Y. Yu, Y. J. Lee, and M. Bauchy, "Intrinsic nano-ductility of glasses: The critical role of composition," *Front. Mater.* **2**(5), 521 (2015).
- ⁵⁴T. To, S. S. Sørensen, Y. Yue, and M. M. Smedskjaer, "Bond switching is responsible for nanoductility in zeolitic imidazolate framework glasses," *Dalton Trans.* **50**(18), 6126 (2021).
- ⁵⁵A. P. Thompson, S. J. Plimpton, and W. Mattson, "General formulation of pressure and stress tensor for arbitrary many-body interaction potentials under periodic boundary conditions," *J. Chem. Phys.* **131**(15), 154107 (2009).
- ⁵⁶F. Shimizu, S. Ogata, and J. Li, "Theory of shear banding in metallic glasses and molecular dynamics calculations," *Mater. Trans.* **48**(11), 2923 (2007).
- ⁵⁷T. Rouxel, "Driving force for indentation cracking in glass: Composition, pressure and temperature dependence," *Philos. Trans. R. Soc., A* **373**(2038), 52 (2015).
- ⁵⁸Z. Zhang and W. Kob, "Revealing hidden medium-range order in silicate glass formers using many-body correlation functions," *Phys. Rev. B* **110**(10), 363 (2024).
- ⁵⁹Z. Zhang, S. Ispas, and W. Kob, "Surface properties of alkali silicate glasses: Influence of the modifiers," *J. Chem. Phys.* **158**(24), 363 (2023).
- ⁶⁰J. D. Mackenzie and R. P. Laforce, "High-pressure densification of glass and the effects of shear," *Nature* **197**(4866), 480 (1963).
- ⁶¹K. Goetzke and H. J. Klein, "Properties and efficient algorithmic determination of different classes of rings in finite and infinite polyhedral networks," *J. Non-Cryst. Solids* **127**(2), 215 (1991).
- ⁶²J. Du and A. N. Cormack, "The medium range structure of sodium silicate glasses: A molecular dynamics simulation," *J. Non-Cryst. Solids* **349**(2), 66 (2004).